Fine-Tuning of Electronic Structure of Cobalt(II) Ion in Nonplanar Porphyrins and Tracking of a Cross-Hybrid Stage: Implications for the Distortion of Natural Tetrapyrrole Macrocyc...

ARTICLE *in* THE JOURNAL OF PHYSICAL CHEMISTRY B · OCTOBER 2015

Impact Factor: 3.3 · DOI: 10.1021/acs.jpcb.5b08431

5 AUTHORS, INCLUDING:

Qiuhua Liu

Hunan University of Science and Technology

8 PUBLICATIONS **67** CITATIONS

SEE PROFILE

Zaichun Zhou

Hunan University of Science and Technology

12 PUBLICATIONS **76** CITATIONS

SEE PROFILE

THE JOURNAL OF PHYSICAL CHEMISTRY B

Article

pubs.acs.org/JPCB

Fine-Tuning of Electronic Structure of Cobalt(II) Ion in Nonplanar Porphyrins and Tracking of a Cross-Hybrid Stage: Implications for the Distortion of Natural Tetrapyrrole Macrocycles

Qiuhua Liu,[†,‡] Xi Zhang,[‡] Wennan Zeng,[‡] Jianxiu Wang,[*,†] and Zaichun Zhou[*,‡]

[†]College of Chemistry and Chemical Engineering, Central South University, Changsha 410083, China

[‡]Key Laboratory of Theoretical Organic Chemistry and Functional Molecule of the Ministry of Education; School of Chemistry and Chemical Engineering, Hunan University of Science and Technology, Xiangtan 411201, China

Supporting Information

ABSTRACT: The core size of the porphyrin macrocycles was closely related to their stability of the different electron structure in the central metal ion. Cobalt(II) ions can undergo a conversion in electron configurations upon N_4 core contraction of 0.05 Å in nonplanar porphyrins, and these ions still maintain low spin forms after and before conversion. The structural fine-tuning can induce the appearance of a cross-hybrid stage $[d(_{x^2-y^2})sp^2 \leftrightarrow d(_{z^2})sp^2]$ based on quadrilateral coordination of the planar core. The results indicate that the configuration conversion plays a key role in electron transfer in redox catalysis involving cobalt complexes. The electronic properties of six monostrapped cobalt(II) porphyrins were investigated by spectral, paramagnetic, and electrochemical methods. The macrocyclic deformations and size parameters of Co-containing model compounds were directly obtained from their crystal structures.

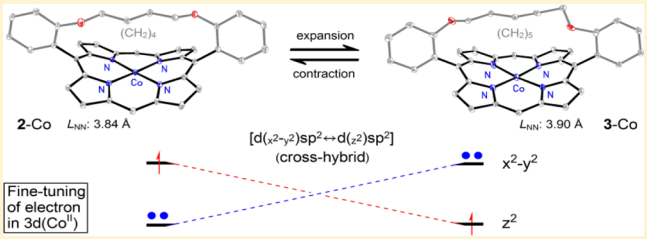

1. INTRODUCTION

Metalloporphyrins are extensively used as catalysts for various organic transformations that are difficult to achieve using regular metal complexes, and this is possible because of their unique structure.[1] Cobalt atom complexes have easily accessible oxidation states of Co(I), Co(II), Co(III),[2] and even Co(IV) and Co(V) under electrochemical conditions.[3] The Co(III)/Co(II) interconversion in porphyrins is readily achieved upon aerobic oxidation[4−6] or mild reduction[7] in high yield. Modified Co(II) porphyrins are efficient and versatile catalysts for the selective olefination of carbonyl compounds[8] and olefin cyclopropanation[9] with suitable diazo compounds. These reactions depend on "cobalt(III)−carbene radicals" for olefin cyclopropanation[10] and "cobalt(III)−nitrene intermediates" for C−H amination.[11]

The macrocycle in coenzyme B_{12}, however, is a confused tetrapyrrole-substituted or reduced, corrole,[12] rather than the classic macrocycle, such as modified porphyrin in heme[13] or chlorophyll.[14] The smaller core size of free corrole compared with that in porphyrin may be crucial for these functions, including the high reactivity and the stability of high valence Co in coenzyme B_{12} and in corrole.[15] The coenzyme B_{12} was observed very early to bring about distortion of the corrole ring system in performing its latent catalysis.[16−18] Recent theoretical studies have suggested that conformational changes in the macrocycle of many enzymes, e.g., heme[19] and cytochrome P450,[20] may play a very important role in their functions. Macrocyclic distortion and the resulting core contraction can result in changes in the electronic[21−23] and magnetic properties[24−26] of the central iron ion[27] and in the nonbinding interaction of the *meso*-aryl.[28] These results imply that the reason "why nature does not use the porphyrin ligand in vitamin B_{12}" is a possible size mismatching of core to Co^{3+} ions rather than sterical inflexibility of the macrocycle.[29]

In a recent report, we clarified the role of macrocyclic deformation modes and of the degree of distortion in heme for a series of ruffle-type porphyrins and a dome-type porphyrin.[30,31] We found a conversion of electronic configuration and the formation of cross-hybrid states in the central iron and zinc ions under core contraction for different nonplanar metalloporphyrins.[32−34] These findings provided experimental support to the assertion that distorted heme can generate and stabilize a high valent iron(V)-oxo complex[35] by a change in its macrocyclic deformations and its related core size.

The core size is smaller in the corrole macrocycle with one less porphyrin *meso*-carbon[36] (Figure 1). For Co(II) porphyrin, the 3.90 Å core diameter (Figure 1, right) is much smaller than the free cavity ($L_{NN} \sim 4.10$ Å) of free base porphyrin, which implies an imperfect size-matching between the diameter of the metallic ion and the macrocyclic core size. A smaller cavity ($L_{NN} < 3.90$ Å) is required to adjust the metal's electronic configuration when complexed with a small ion, such as

Received: August 29, 2015
Revised: October 13, 2015
Published: October 13, 2015

DOI: 10.1021/acs.jpcb.5b08431
J. Phys. Chem. B 2015, 119, 14102−14110

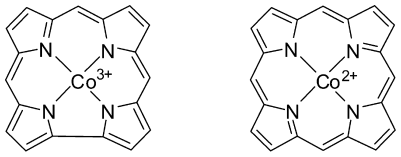

Figure 1. Core size comparison between Co(III) corrole (left)[37,38] and Co(II) porphyrin (right).[40,41] L_{NN} is core diameter represented by the average length of the diagonal N atoms in the macrocyclic center.

Co(II).[37] The crystal structure of Co(III) corrole reveals that the core ion can be compressed to 3.78 Å (Figure 1, left);[38] this value is very close to that in natural cobalamin.[39] These results indicate that the corrole has a smaller cavity and can stabilize a higher valence form compared with that in porphyrin upon the inclusion of cobalt ions.

It has been reported that corrole macrocycles stabilize the Co(III) oxidation state whereas porphyrins mainly stabilize cobalt ions in the lower valence Co(II) form.[42,43] We are interested in whether the Co(II) ions can be regulated by core contraction to stabilize at another electronic state or at higher oxidation states and display a high reactivity like those in corroles if the porphyrin core is contracted to small enough.

In this report, we show experimentally that the macrocyclic deformation of porphyrins can induce a conversion of electronic structure in the central cobalt(II) ion and achieve a cross-hybrid coordination $[d(_{x^2-y^2})sp^2 \leftrightarrow d(_{z^2})sp^2]$ based on N_4 core and can thus activate the only odd electron in its $3d_{z^2}$ orbital upon a compression of the core size. A highly deformed porphyrin can perform a trigger function because of this core contraction. The electronic properties of cobalt ions in porphyrins have been studied by spectral, paramagnetic and electrochemical methods, and the structural parameters of the model compounds can be directly obtained from their crystal structures.

2. RESULTS AND DISCUSSION

One series of monostrapped nonplanar metalloporphyrins, as their cobalt complexes **1**-Co to **6**-Co (Scheme 1), were selected

Scheme 1. Model Compounds[a]

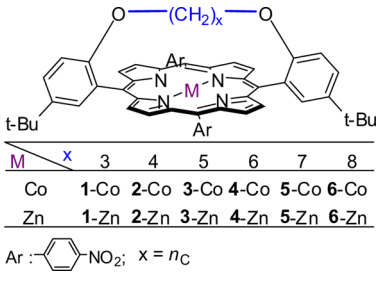

[a]Zinc complexes **1**-Zn to **6**-Zn are selected as baseline complexes of cobalt porphyrins **1**-Co to **6**-Co. n_C is the number of carbon atoms in straps.

as model systems for the above-mentioned targets. These strapped porphyrins provide samples with a reliable deformation mode and continuous distortion degree, and they are capable of producing more sufficient distortion than that in early basket handle ones.[44] These model complexes were prepared and characterized according to our previous report.[32,45] Their zinc complexes, **1**-Zn to **6**-Zn, were used as baseline objects.

2.1. Spectral Analysis. The distortion of porphyrin macrocycles is known to result in a spectral red shift.[30,31,46] For the zinc porphyrins **1**-Zn to **6**-Zn, the electronic spectra showed a regular red shift as the degree of distortion increased.[30,34] For the cobalt porphyrins **1**-Co to **6**-Co, however, the spectral shift was not continuous, and an inflection point was present at n_C = 5. (Figure 2).

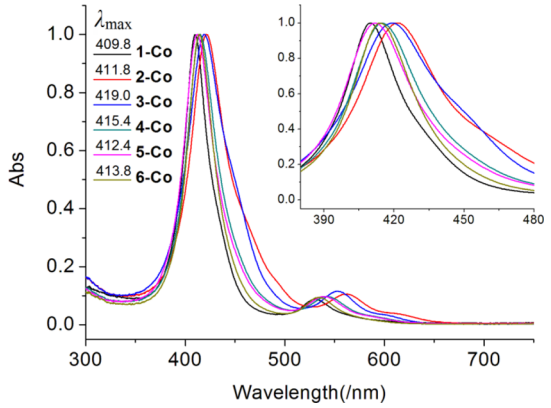

Figure 2. Absorption spectra of the strapped cobalt porphyrins **1**-Co to **6**-Co in $CHCl_3$ (~2.0×10^{-6} M) at 293 K.

The spectral shift of the distorted porphyrins indicates a change at the molecular level of the ground state,[32,34] and this provides a means of determining the electronic properties and coordination behavior of the central metal ion. The differential spectra method can be used to track changes in the energy levels of these metalloporphyrins, as discussed in our previous report.[32,33] The spectral shifts are dependent on the size difference between the metallic ions.[47] In line with the rule for strapped iron porphyrins, a conversion was also evident in the absorptive spectra of the series of Co-containing porphyrins (Figure 3).[48] The conversion point is at n_C = 5 rather than at n_C = 4 as was found for the iron porphyrins, and the deviation range is much larger than those in the spectra of the iron analogues. The differential value, $\Delta\lambda_{max}$, represents the spectral shift between the cobalt porphyrins and their corresponding zinc porphyrins. For **3**-Co to **6**-Co, a regular red shift was found for a low degree of distortion ($n_C \geq 5$) in their electronic spectra whereas those of compounds **1**-Co and **2**-Co exhibited an ~18 and ~10 nm deviation from the extended trend line based on the curve for **3**-Co to **6**-Co.

The higher $\Delta\lambda_{max}$ value and the spectral deviation come from the larger change in the ground state energy level (ΔE) compared with those of the iron porphyrins. From the graph, the curve can also be divided into two sections similar to that in strapped iron porphyrins under core contraction (labeled a and b, Figure 3). The molecular energy level mainly depends on the macrocyclic deformation or the core size change. This spectral deviation indicates an increase of >10 kJ/mol for the energy level, which implies that the macrocyclic out-of-plane deformation is visibly weakened and the spectral red shift decreases while the in-plane deformation is relatively strengthened. The spectral blue shift increases because of the resultant small size of low spin Co(II) after the conversion.[32] These spectral shifts and changes in the energy level indicate that the conversion of configuration requires the macrocycle to

DOI: 10.1021/acs.jpcb.5b08431
J. Phys. Chem. B 2015, 119, 14102−14110

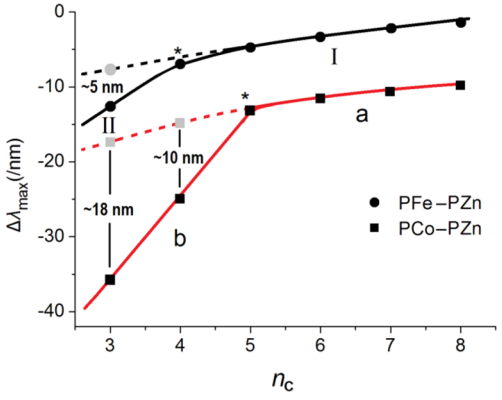

Figure 3. Differential spectra comparison at Soret band between the strapped cobalt porphyrins **1**-Co to **6**-Co (red line) and the corresponding zinc complexes **1**-Zn to **6**-Zn at the Soret band in a $CHCl_3$ solution (~2.0 × 10^{-6} M) at 293 K. $\Delta\lambda_{max}$ is the spectral shift of the maxima for each cobalt porphyrin (e.g., **1**-Co) and its corresponding zinc analogue (**1**-Zn). The dotted line represents the predicted trend based on the same hybrid mode of the N_4 core as that in those with a more planar macrocycle. The $\Delta\lambda_{max}$ of the iron analogues **1**-Fe to **6**-Fe (black line) is taken from our previous report.[32,33]

possess a smaller N_4 cavity and that the formation of a cross stage requires a far higher energy than that of the starting state with low distortion.

2.2. Structural Analysis. The spectral visible deviation implies a discontinuous macrocyclic deformation of the model cobalt porphyrins **6**-Co to **1**-Co, that is, a discontinuous trend for their core sizes as their straps continuously shorten. An earlier report demonstrated that the porphyrin core can be expanded or contracted by regulating the spin state of the nickel(II) ion within the porphyrin.[49,50] The crystal structures of the model compounds **1**-Co to **4**-Co around the conversion position in spectral graph (Figure 3) were obtained to determine the change in core size. The cavity parameters for the four compounds, **1**-Co to **4**-Co, are shown in Figure 4.

The macrocycles of the four Co-containing complexes, **1**-Co to **4**-Co, adopted a ruffle-like deformation, and the core size does not decrease systematically as the straps are shortened.[31]

The core size trend reveals that the core diameter of the four macrocycles has two independent magnitudes, as shown by a plot of L_{NN} against n_C (Figure 5). The core diameters of

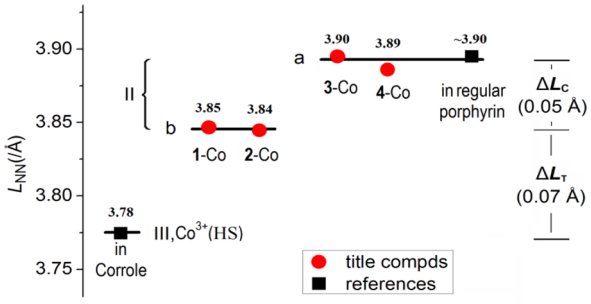

Figure 5. Comparison of core diameter (L_{NN}) in the strapped compounds **1**-Co to **4**-Co to that in references. ΔL_C denotes the difference value of core diameter in between states a and b accommodating Co(II) ions, and ΔL_T is that in between states b and Co(III) ions.

complexes **3**-Co and **4**-Co are very close (L_{NN} = 3.89–3.90 Å), and their values are almost the same as that (~3.90 Å) in the regular porphyrin system.[39] This magnitude implies an independent state (labeled a, Figure 5), while the diameters of compounds **1**-Co and **2**-Co are 3.84–3.85 Å, which is significantly smaller than the above-mentioned diameters and can be assigned to another state (b, Figure 5). The two states are in line with those which take place in the spectral trend line (sections a and b, Figure 3). The diameter (~3.85 Å) of state b visibly deviates from that (~3.90 Å) of state a; the deviation value (ΔL_C) of both is 0.05 Å, and it approaches the core diameter (3.78 Å) of corrole whose central cobalt species belongs to the high spin Co(III) ion, with a difference (ΔL_T) of 0.07 Å. Note that, for the current four structures, the error of the Co–N bond is in the range 0.003–0.006 Å (Table 1 and Supporting Information p S2): the error is much smaller than the 0.05 Å of the ΔL_C between state a and state b.

One other thing to note is the difference of axial coordination in the **2**-Co structure from those in the other three. Specifically, the **2**-Co structure has no axial ligand,

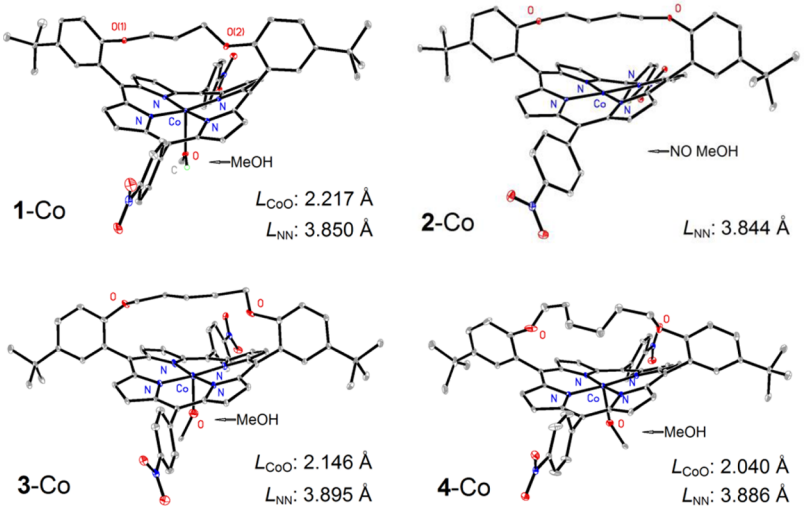

Figure 4. Crystal structures of strapped cobalt porphyrins, **1**-Co to **4**-Co (straps are $O(CH_2)_xO$, x = 3–6, respectively). L_{CoO} denotes the distance of central Co to O in methanol as ligand, with the symbol L_{NN} being described in Figure 1. All protons have been omitted for clarity.

DOI: 10.1021/acs.jpcb.5b08431
J. Phys. Chem. B 2015, 119, 14102–14110

Table 1. Selected Bond Lengths (L_{CoN}) and Atom Distances (L_{NN}) for Different Co Ion Forms

Co forms	Co(II) (**2**-Co)	Co(II) (**3**-Co)	Co(II)[b]	Co(III)[c]
L_{NN}[a]/Å	3.84	3.90	3.90	3.78
L_{CoN}[a]	1.919(6)	1.950(5)	1.934(3)	1.888(3)
$L_{CoN(1)}$	1.921(6)	1.940(5)	1.949(3)	1.879(3)
$L_{CoN(2)}$	1.914(6)	1.958(5)	1.946(3)	1.900(3)
$L_{CoN(3)}$	1.917(6)	1.973(5)	1.947(4)	1.894(3)
$L_{CoN(4)}$	1.922(6)	1.929(5)	1.946(3)	1.878(3)

[a]L_{CoN} represents the averaged bond length between Co and N in the macrocyclic center. L_{NN} is described in Figure 1. [b]The distance parameters are from its regular porphyrin complex,[41] and the values will be slightly shortened in the absence of axial ligand.[40] [c]The parameters are from Co(III)[38] corrole complex.

methanol, while the other three do. This difference brings about two questions: why it occurs and how much of an impact on the molecular structure it will produce. For the first question, the cobalt ion is in the edge of state conversion in the **2**-Co structure; its electronic structure as metastable state is reluctant to convert, which disturbs the potentially empty orbital to stabilize the axial ligand, whereas the ion in the other three is in a stable state based on a complete conversion and its axial coordination is also stable. The more evident twin crystal phenomenon in **2**-Co can support the analysis (see Supporting Information p S3). As for the second question, the impact of the axial methanol on molecular structure in current system should be very tiny. An additional explanation is placed in Supporting Information (p S4).

The diameter of cobalt ions (d_{Co}) evidently relies on their chemical valence and electronic structure under the same coordination surrounding according to the Shannon effective ionic radii table[51] (Figure 6). For the Co^{2+} ion, the difference

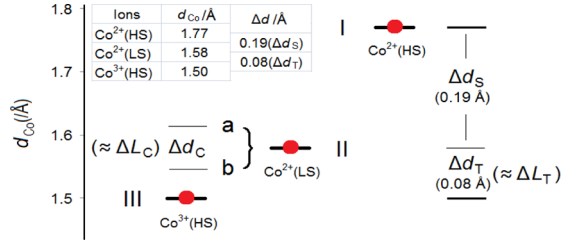

Figure 6. Comparison of ionic diameter (d_{Co}) of cobalt in three states. The values in the inset table include the ionic diameters of six-coordinated cobalt ions according to the Shannon effective ionic radii table;[50] Δd_S is the difference value in diameter between HS and LS of Co(II) ion, and Δd_T is that between LS Co(II) and HS Co(III) ion based on electron transfer.

value in diameter can be up to 0.19 Å (Δd_C) between its two spin forms of high and low spin. As far as the Co^{3+} ion is concerned, its diameter is smaller than that of the low spin Co^{2+} ion, and the difference value of the both is 0.08 Å (Δd_T). In other words, the spin decrease of the Co(II) ion would produce (or need) the 0.19 Å contraction of the macrocyclic core, and the output of one electron will only lead to the 0.08 Å contraction.

Two size transition stages take place on the basis of the three states in Figures 5 and 6. In theory, the change in core diameters (ΔL) in macrocycles should be equal (or close) to the change in ionic diameters (Δd) if this change was based on the same conversion of ion forms. The facts, however, are not exactly like that. The latter two (ΔL_T and Δd_T) are highly consistent: both are 0.07 and 0.08 Å, respectively. The electron transfer process is in line with the change of cobalt ions in diameter, so it can be reasonably believed that the core contraction of the model macrocycles naturally results in the electron output (state b to state III in Figure 5). The ~3.85 Å of core size represents a critical size for conversion from the low spin Co(II) ion to the high spin Co(III) ion, whereas the former two (ΔL_C and Δd_S) are not consistent, ΔL_C = 0.05 Å, and Δd_S = 0.19 Å, their difference is up to 0.14 Å. The conversion (from state a to b) of electronic configuration in the current cobalt series, however, is not analogous to spin conversion in strapped iron porphyrins [from intermediate spin (IS) to low spin (LS)] under core contraction.[33] The states a and b could only belong to two subforms of low spin Co(II) ions (Figure 6), and the fine deviation of 0.05 Å (ΔL_C) is possibly derived from the difference (possible Δd_C) of two subforms in size. The electronic structures of two states a and b need further experimental support.

2.3. Electron Paramagnetic Resonance Analysis. The configuration conversion, that is, an electronic tautomerism of central ions, leads to a visible change in other spectral properties such as the electron paramagnetic resonance (EPR)[52−54] besides the above absorptive spectra.[32] The EPR technique can effectively track the behaviors of unpaired electrons in Co(II) porphyrins.[55] In this section, an EPR experiment was performed to follow the change of electronic structure in cobalt(II) ion. The EPR measurements were obtained in a toluene solution (~3 mM) of **1**-Co to **6**-Co at 130 K under an inert gas after degas on a vacuum line. The EPR results are shown in Figure 7.

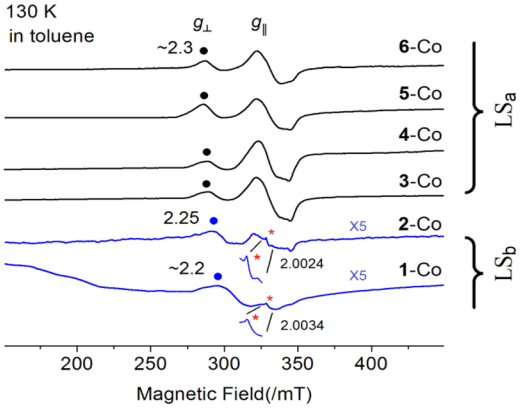

Figure 7. EPR spectra of cobalt complexes **1**-Co to **6**-Co in toluene solution (~3.0 × 10^{-3} M) at 130 K after deoxygen treatment. The inserts indicated with asterisks (*) are the magnified radical signals. These spectra were recorded with a microwave power of 998 μW at 9.0408 GHz, a modulation amplitude of 0.25 mT, and a modulation frequency of 100 kHz.

A small variation of the macrocycle can induce marked changes in heme chemistry because of the high flexibility of the macrocycle.[56] Reports showed that the low spin iron(III) ion can vary in the different electronic ground states by virtue of the deformations of porphyrin.[57−59] This phenomenon can also take place in the current model system containing Co(II) ion. EPR parameters are directly compared to those of other Co(II) porphyrins reported.[55,60] If five-coordinate Co(II) ion complexes have *g*-values 8.6, 1.3, and 0.9 for high spin species,[61] then *g*-values 2.2−2.3 and 2.0 are low spin.[55,60] The EPR results

DOI: 10.1021/acs.jpcb.5b08431
J. Phys. Chem. B 2015, 119, 14102−14110

for all six Co-containing compounds are consistent with a low spin (LS) d^7 Co(II) feature, rather than the high spin one, although the signals show a slight shift. Still, the EPR signals also display some differences in the $g_{\|}$ branch, which can imply a conversion in electronic structure of the Co(II) ion. Four samples, **3**-Co to **6**-Co, have a typical low spin (LS) Co(II) feature ($g_{\perp}$ 2.26, and $g_{\|}$ 2.0).[62] However, for two other samples, **1**-Co and **2**-Co display much weaker $g_{\perp}$ and $g_{\|}$, and include a visible radical signal (labeled by red *) in the $g_{\|}$ branch. The branch containing free radical signal in EPR spectra of **1**-Co and **2**-Co indicates a mixing of two states at least, a new low spin Co(II) and a radical. The new low spin Co(II) is derived from electron exchange discussed above, and the radical is from the formation of an activated state $Co(III)^{\bullet+}$ complex as cation radical, which is supported by the early report.[63] The EPR spectra are significantly split after this core contraction. The former $g_{\perp}$ value denotes a low spin d^7 with the odd electron in the d_{z^2} orbital,[55] which means that the odd electron in compounds **3**-Co to **6**-Co still stays in the d_{z^2} orbital, whereas that in **1**-Co and **2**-Co is transferred to other orbitals or positions. The six samples can also be divided into two types (a and b in Figure 7) according to the EPR difference.

The 3d orbital of low spin Co(II) ion has an orbital splitting (Figure 8, right) in an axial symmetric hybrid mode.[64] For

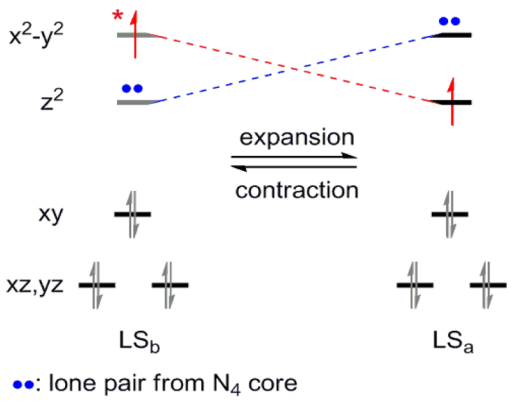

Figure 8. 3d orbital splitting of Co(II) ions before (right) and after (left) core contraction. * represents an activated electron.

compounds **3**-Co to **6**-Co, they possess the typical electron arrangement of axial symmetric field before core contraction (L_{NN} ~ 3.90 Å). The sole odd electron stays in the d_{z^2} orbital with a lower energy level than the $d_{x^2-y^2}$ one, and it is compelled to a higher $d_{x^2-y^2}$ orbital after core contraction (Figure 8, left). In other words, the positions of the odd electron and a lone pair from the N_4 core are entirely exchanged between the $3d_{z^2}$ and $3d_{x^2-y^2}$ orbitals under the potent core change in size evidenced in the analogue of iron-containing complexes.[32,33] The coordination mode of the N_4 core will change from the $d(_{z^2})sp^2$ form to the $d(_{x^2-y^2})sp^2$ one, which is necessary for the experience of a cross-hybrid stage [$d(_{x^2-y^2})sp^2 \leftrightarrow d(_{z^2})sp^2$]. EPR spectra also indicate that the valences and spin types of the Co(II) ions remain unchanged in title cobalt complexes, while their electronic configurations are converted during the fine core change. These facts, the unstable coordination of apical position and more evident twin crystal phenomenon in **2**-Co structure, can also support the occurrence of the cross-hybrid stage. During the course of this exchange, the electron in the d_{z^2} orbital is activated. The radical signal originates from the delocalization of the activated odd electron in a large π system.

For iron(III) porphyrins, it was found that the metallic ion can undergo a core contraction of 0.01−0.03 Å under the electron transfer process from the $3d_{z^2}$ orbital to the $3d_{x^2-y^2}$ one.[32,33] So, the fine deviation of 0.05 Å (ΔL_C) in the above structures can be assigned the difference (Δd_C) between two low spin subforms a and b of the cobalt(II) ion.

Molecular dioxygen is of high sensibility to the unpaired electron in the d orbital.[54] In this case, the dioxygen molecule should be of a higher sensibility to the unpaired electron in the d_{z^2} orbital than that in the $d_{x^2-y^2}$ one and forms the more stable O_2-containing complex. A control experiment was performed to follow the change of electronic structure in the cobalt(II) ion in the presence of oxygen and to observe the effect of its odd electron on dioxygen under core contraction. The new EPR results are displayed in Figure 9.

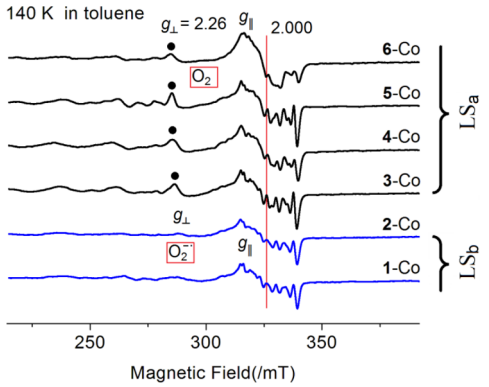

Figure 9. EPR spectra of cobalt porphyrins **1**-Co to **6**-Co in toluene solution (~3.0×10^{-3} M) at 140 K in the presence of oxygen. These spectra were recorded under the same conditions as those in Figure 7.

The Co−O_2 complexes mainly observed in the EPR spectra of the **3**-Co to **6**-Co complexes are converted to a possible $Co(II)-O_2^{\bullet-}$ radical form of the **1**-Co to **2**-Co ones under core contraction, which is manifest as disappearance of the $g_{\perp}$ signal (Figure 9). It is simply the case that the radical complex is much more stable for the **1**-Co and **2**-Co complexes than that for the **3**-Co to **6**-Co ones, and so the $g_{\perp}$ branch in EPR spectra of **1**-Co and **2**-Co complexes bound to O_2 cannot be seen, while the $g_{\|}$ branch is buried under the part which is the O_2 complex spectrum. Each of eight-line hyperfine patterns ($g_{\|}$) that feature around ~2.0 is derived from the further split by a hyperfine interaction with a dioxygen.[65,66] These facts indicate the rise of energy level of the $3d_{x^2-y^2}$ orbitals, which assures enough activity of the odd electron. This confirms that a new LS Co(II) species takes place in the **1**-Co and **2**-Co porphyrins. This conclusion means that the ~3.90 Å of core size only represents a critical size for the electron exchange in the low spin Co(II) ions. This comparative analysis indicates that it is the core contraction that promotes the conversion of electronic structures (electron exchange) for the LS Co(II) ions of the title models. Unfortunately, The Co−O_2 binding cannot be directly observed in the relevant crystal structures of Co complexes as is taking place in the previous Zn−O_2 system,[34] which may be limited by the weak binding in the current Co−O_2 component.

2.4. Electrochemical Analysis. Porphyrin nonplanarity induced by protein can represent a new strategy to rationally tune the redox properties of the central metal.[67] The electrochemical properties of metalloporphyrins in nonaqueous

DOI: 10.1021/acs.jpcb.5b08431
J. Phys. Chem. B 2015, 119, 14102−14110

media had been reviewed.[68] The cyclic voltammograms of the model compounds (~3.0 mM) were obtained in benzonitrile solution including 0.1 M *tetra-n*-butylammonium hexafluorophosphate ($TBAPF_6$) at room temperature, and the scan rate is 0.1 V/s. The electrochemical results are given in Figure 10.

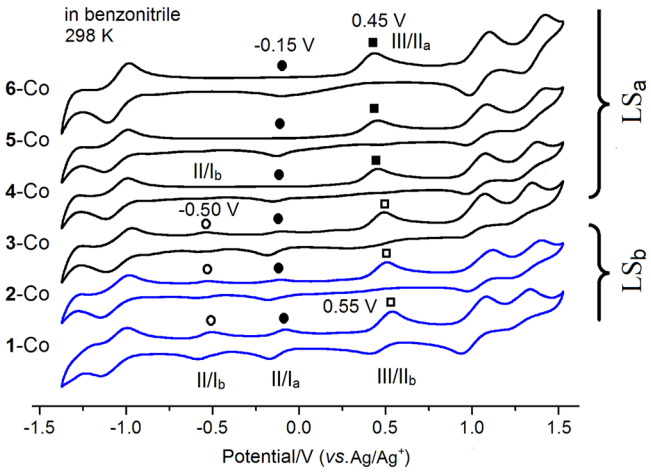

Figure 10. Cyclic voltammograms of compounds **1**-Co to **6**-Co in an inert atmosphere at room temperature in benzonitrile containing 0.1 M $TBAPF_6$ as supporting electrolyte. Scan rate = 0.1 V/s. The inset is the voltage of the oxidation peak (E_p), rather than the half-wave voltages ($E_{1/2}$), for electron couples II/I and III/II, respectively.

A cyclic voltammogram of regular cobalt porphyrins adsorbed onto a graphite disk shows two reversible processes at oxidation and reduction half-wave voltages ($E_{1/2}$) of 0.60−0.80 and −0.20 V.[10,69] These are assigned to two reactions based on the electron couples Co(III)/Co(II) and Co(II)/Co(I), respectively. One of the well-resolved electrochemical responses in compounds **1**-Co to **6**-Co appears in the range 0.45−0.55 V (Figure 10, indicated by tilted squares) shown as the voltage of the oxidation peak (E_p). Also, the value can be assigned to the Co(III)/Co(II) reaction, while for the Co(II)/Co(I) reaction, the responses for these Co-containing complexes reveal different rules for core contraction. A signal splitting phenomenon occurs at the Co(II)/Co(I) branch for **1**-Co to **3**-Co; that is, a new response appears at the position of −0.50 V (labeled by ○) besides the normal one of −0.15 V (labeled by ●), which is consistent with the values reported.[10] According to the difference of electrochemical branch, the six samples could also be divided into two classes, **1**-Co to **3**-Co, and **4**-Co to **6**-Co. We will now discuss the origin of the new response at −0.50 V in the Co(II)/Co(I) branch. In more planar macrocycles, an electron pair from the N_4 core occupies a higher $3d_{x^2-y^2}$ orbital, which induces the response of the electron in the $3d_{z^2}$ orbital (labeled by red *, Figure 11, left) to appear at normal position (II/I_a) of −0.15 V. However, in more deformed macrocycles, the electron pair of the N_4 core intrudes into the lower $3d_{z^2}$ orbital, and that odd electron (marked with a red) initially occupying the $3d_{z^2}$ one is compelled to the empty $3d_{x^2-y^2}$ orbital and is activated. The reduction potential of the activated electron will appear at a more negative position (II/I_b) compared to the initial one (II/I_a) before activation. So, the signal splitting can be attributed to the exchange of electron pair between the $3d_{z^2}$ and $3d_{x^2-y^2}$ orbitals after sufficient core contraction, and the Co(II) species can undergo two types of redox reactions in compounds **3**-Co to **1**-Co. The signal

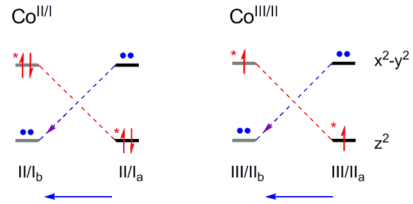

Figure 11. Schematic of the electron configuration of Co ion in the cyclic voltammetric analyses. The blue arrows represent the direction of core contraction, and the red stars (*) are the electrons transferred on the basis of the related electrochemical reaction.

splitting of samples **1**-Co to **3**-Co also implies a coexistence of the $d(_{x^2-y^2})sp^2$ hybrid and $d(_{z^2})sp^2$ ones based on quadrilateral coordination of the planar N_4 core. The coexistence can be defined as a cross-hybrid stage $[d(_{x^2-y^2})sp^2 \leftrightarrow d(_{z^2})sp^2]$.

For the same reason, the similar splitting phenomenon also should happen in the Co(III)/Co(II) reaction branch because of the electron exchange (III/II_a and III/II_b, Figure 11, right) as discussed above.[70] We thought that the phenomenon also exists. For samples **1**-Co to **6**-Co, the well-resolved electrochemical responses also appear in the two isolated ranges of ~0.45 and ~0.55 V (Figure 10, indicated by ■ and □, respectively); both can been assigned to the III/II_a and III/II_b forms of the Co couple above, respectively. Unlike the Co(II)/Co(I) reaction, no coexistence of $d(_{x^2-y^2})sp^2$ hybrid and the $d(_{z^2})sp^2$ one takes place in the Co(III)/Co(II) reaction, which implies a short stage of cross-hybrid $[d(_{x^2-y^2})sp^2 \leftrightarrow d(_{z^2})sp^2]$. This is because the potentials for the Co(III)/Co(II) electrode reaction should shift to a more negative value from **6**-Co to **1**-Co based on the increase of the electron density on the central metal ion during core contraction. In the current measurement, the change trend of potentials goes by, as shown as a positive shift from 0.45 to 0.55 V. This positive shift can be attributed to different electrochemical responses of the central metal ion during core contraction. According to the structural and spectral information on the models above, the splitting phenomenon is only included in the measurement of **2**-Co and **1**-Co. It is believed that the thermal movement (possibly including the ionic enlargement for Co(I) species) drives the signal splitting to occur in a more planar system, **3**-Co.

■ CONCLUSIONS

In conclusion, low spin Co(II) ions can be used to generate electronic tautomerism upon sufficient core contraction in nonplanar porphyrins because of the activation of odd electron in the $3d_{z^2}$ orbital. Our findings reveal that the core size of macrocycles is closely related to the stability of the different electronic structure and valence states of the central cobalt ions, and the structural fine-tuning plays a possible mechanochemical trigger role in performing the electron transfer in catalysis involving transition metal complexes in Co(II) porphyrin. The findings afford another direct experiment material for the cross-hybrid concept initially defined in our previous report. The data also provides an insight into the unique biochemical functions of corrole with a smaller core than porphyrin in coenzyme B_{12}. This is helpful in understanding the significance of core size in the redox catalysis of porphyrin-like complexes in living systems.

DOI: 10.1021/acs.jpcb.5b08431
J. Phys. Chem. B 2015, 119, 14102−14110

MATERIALS AND METHODS

Reagent grade reactants and solvents were used as received from chemical suppliers. Cobalt insertion leading to the model Co-containing species was carried out under a standard method. UV−vis spectra were recorded on a PerkinElmer Lambda 35. Routine ^{1}H NMR spectra were obtained at ambient temperature on a Bruker AV II 500 MHz spectrometer using deuterated chloroform solutions with $CHCl_3$ (δ = 7.26 ppm) as an internal standard. Mass spectra were measured with a Varian QFT-ESI mass spectrometer. EPR spectra were obtained on a JEOL JES-FA200 EPR spectrometer (140 K and room temperatures, 9.0408 GHz, X band). The cyclic voltammogram results were obtained on a CHI760E electrochemical workstation (Autolab) with a glass carbon electrode as the working electrode, a platinum wire as counter electrode, and Ag/Ag^+ as reference electrode. Infrared spectra were recorded on a FTIR PerkinElmer 1600 spectrometer.

Crystal structure determination by X-ray diffraction was performed on a Bruker SMART 1000 CCD diffractometer equipped with a normal focus, 2.4-KW sealed-tube X-ray source using monochromatic Mo Kα (λ = 0.710 73 Å) radiation. A suitable single crystal of each compound was carefully selected and glued to a thin glass fiber with superglue adhesive. The SMART program package was used to determine the unit-cell parameters and for data collection. All structures were solved by direct methods and refined on F^2 by full-matrix least-squares using the SHELXT-97 program system. The positional parameters for metal, N, and O atoms were located by direct methods for all compounds. The remaining non-hydrogen atoms were routinely located from Fourier difference maps during the course of the refinement. All the hydrogen positions were placed geometrically with refinement by riding on their appropriate O and C atoms. The final positions of all non-hydrogen atoms were refined anisotropically.

The target nonplanar cobalt porphyrins **1**-Co to **6**-Co and zinc complexes **1**-Zn to **6**-Zn were prepared according to our previous reports,[43,31] and their crystals were obtained by the solvent diffusion method in chloroform and methanol. General method follows: solid cobalt acetate (~0.5 g) was added to 50 mL of DMF solution of free base porphyrin **1** (or **2**−**6**, 49−52 mg). The resulting solution was stirred for 6 h at refluxing condition, poured into 120 mL of water, and filtered, and then the residue solid was dissolved with chloroform (30 mL × 3), and dried over sodium sulfate. The residue was separated by silica gel column chromatography with EA/PE (1:5; V/V) to afford **1**-Co (or **2**-Co−**6**-Co) as purple solids in yield 85−95%.

Compound **1-Co**, 53.5 mg, yield in 84.0%. UV−vis (chloroform, 293 K) λ_{max}: 409.8, 530.0, 572.8 nm. ESI-HR MS m/z (%), Calcd for $[C_{55}H_{46}CoN_6O_6]^+$ = 945.2805. Found: 945.2811.

Compound **2-Co**, 54.5 mg, yield in 85.6%. UV−vis (chloroform, 293 K) λ_{max}: 421.8, 566.6, 610.5 nm. ESI-HR MS m/z (%), Calcd for $[C_{56}H_{48}CoN_6O_6]^+$ = 959.2962. Found: 959.2968.

Compound **3-Co**, 54.8 mg, yield in 86.2%. UV−vis (chloroform, 293 K) λ_{max}: 419.0, 552.2, 592.4 nm. ESI-HR MS m/z (%), Calcd for $[C_{57}H_{50}CoN_6O_6]^+$ = 973.3118. Found: 973.3125.

Compound **4-Co**, 55.1 mg, yield in 86.8%. UV−vis (chloroform, 293 K) λ_{max}: 415.4, 541.2, 578.7 nm. ESI-HR MS m/z (%), Calcd for $[C_{58}H_{52}CoN_6O_6]^+$ = 987.3275. Found: 987.3282.

Compound **5-Co**, 55.5 mg, yield in 87.4%. UV−vis (chloroform, 293 K) λ_{max}: 412.4, 540.0, 576.5 nm. ESI-HR MS m/z (%), Calcd for $[C_{59}H_{54}CoN_6O_6]^+$ = 1001.3431. Found: 1001.3439.

Compound **6-Co**, 55.8 mg, yield in 88.0%. UV−vis (chloroform, 293 K) λ_{max}: 413.8, 535.4, 571.1 nm. ESI-HR MS m/z (%), Calcd for $[C_{60}H_{56}CoN_6O_6]^+$ = 1015.3588. Found: 1015.3592.

ASSOCIATED CONTENT

Supporting Information

The Supporting Information is available free of charge on the ACS Publications website at DOI: 10.1021/acs.jpcb.5b08431.

Systematic characterization (PDF)
Crystallographic data for **1**-Co (CIF)
Crystallographic data for **2**-Co (CIF)
Crystallographic data for **3**-Co (CIF)
Crystallographic data for **4**-Co (CIF)

AUTHOR INFORMATION

Corresponding Authors

*E-mail: jxiuwang@csu.edu.cn.
*E-mail: zhouzaichun@hnust.edu.cn.

Author Contributions

The manuscript was written through contributions of all authors. All authors have given approval to the final version of the manuscript. Q.L., J.W., and Z.Z. contributed equally.

Funding

This work was supported by the National Natural Science Foundation of China (Nos. 21575166, 21372069), and the Natural Science Foundation of Hunan Province, China (No. 13JJ3087).

Notes

The authors declare no competing financial interest.

ACKNOWLEDGMENTS

Prof. Jiafu Chen of University of Science and Technology of China is also acknowledged for his valuable help.

REFERENCES

(1) Meunier, B. Metalloporphyrins as Versatile Catalysts for Oxidation Reactions and Oxidative DNA Cleavage. *Chem. Rev.* **1992**, *92*, 1411−1456.
(2) Vasilevskis, J.; Olson, D. C. Cyclic Amine Complexes of Cobalt(I), -(II), and -(III). Electrochemistry, Preparation, and Properties. *Inorg. Chem.* **1971**, *10*, 1228−1235.
(3) Byrne, E. K.; Theopold, K. H. Redox Chemistry of Tetrakis(1-norbornyl)cobalt. Synthesis and Characterization of a Cobalt(V) Alkyl and Self-exchange Rate of a Co(III)/Co(IV) Couple. *J. Am. Chem. Soc.* **1987**, *109*, 1282−1283.
(4) Tse, A. K. S.; Mak, K. W.; Chan, K. S. Synthesis of Novel Cobalt(III) Porphyrin-Phosphoryl Complexes. *Organometallics* **1998**, *17*, 2651−2655.
(5) Datta-Gupta, N. Preparation and Spectra of Some Cobaltic Complexes of Meso-tetra-p-tolylporphin. *J. Inorg. Nucl. Chem.* **1971**, *33*, 4219−4225.
(6) Ji, L.; Liu, M.; Hsieh, A. K.; Hor, T. S. A. Metalloporphyrin-catalyzed Hydroxylation of Cyclohexane with Molecular Oxygen. *J. Mol. Catal.* **1991**, *70*, 247−257.
(7) Setsune, J.-I.; Ito, S.; Takeda, H.; Ishimaru, Y.; Kitao, T.; Sato, M.; Ohya-Nishiguchi, H. Reversible Complexation of Acetylene with (Perchlorato)cobalt(III) Porphyrins to Form a Novel Dicobalt(II)

DOI: 10.1021/acs.jpcb.5b08431
J. Phys. Chem. B 2015, 119, 14102−14110

Bis(porphyrin) with a Vinylene-N,N′ Linkage. *Organometallics* **1997**, *16*, 597−605.
(8) Lee, M.-Y.; Chen, Y.; Zhang, X. P. General and Selective Olefination of Aldehydes and Ketones Catalyzed by a Cobalt(II) Porphyrin Complex. *Organometallics* **2003**, *22*, 4905−4909.
(9) Dzik, W. I.; Xu, X.; Zhang, X. P.; Reek, J. N. H.; de Bruin, B. 'Carbene Radicals' in CoII(por)-Catalyzed Olefin Cyclopropanation. *J. Am. Chem. Soc.* **2010**, *132*, 10891−10902.
(10) Lu, H.; Dzik, W. I.; Xu, X.; Wojtas, L.; de Bruin, B.; Zhang, X. P. Experimental Evidence for Cobalt(III)-Carbene Radicals: Key Intermediates in Cobalt(II)-Based Metalloradical Cyclopropanation. *J. Am. Chem. Soc.* **2011**, *133*, 8518−8521.
(11) Lyaskovskyy, V.; Suarez, A. I. O.; Lu, H.; Jiang, H.; Zhang, X. P.; de Bruin, B. Mechanism of Cobalt(II) Porphyrin-Catalyzed C−H Amination with Organic Azides: Radical Nature and H-Atom Abstraction Ability of the Key Cobalt(III)−Nitrene Intermediates. *J. Am. Chem. Soc.* **2011**, *133*, 12264−12273.
(12) Abeles, R. H.; Dolphin, D. The Vitamin B_{12} Coenzyme. *Acc. Chem. Res.* **1976**, *9*, 114−120.
(13) Loew, G. H.; Harris, D. L. Role of the Heme Active Site and Protein Environment in Structure, Spectra, and Function of the Cytochrome P450s. *Chem. Rev.* **2000**, *100*, 407−419.
(14) Aronoff, S. The Absorption Spectra of Chlorophyll and Related Compounds. *Chem. Rev.* **1950**, *47*, 175−195.
(15) Li, D.; Stuehr, D. J.; Yeh, S. R.; Rousseau, D. L. Heme Distortion Modulated by Ligand-protein Interactions in Inducible Nitric-Oxide Synthase. *J. Biol. Chem.* **2004**, *279*, 26489−26499.
(16) Barian, V.; Pattridge, K. A.; Lennon, B. W.; Huddler, D. P.; Matthews, R. G.; Ludwig, M. L. Domain Alternation Switches B(12)-Dependent Methionine Synthase to the Activation Conformation. *Nat. Struct. Biol.* **2002**, *9*, 53−56.
(17) Marzilli, L. G.; Toscano, P. J.; Randaccio, L.; Bresciani-Pahor, N.; Calligaris, M. An Unusually Long Cobalt-Carbon Bond. Molecular Structure of trans-Bis(dimethylglyoximato) (isopropyl) (pyridine)-cobalt(III). Implications with Regard to the Conformational Trigger Mechanism of Cobalt-Carbon Bond Cleavage in Coenzyme B_{12}. *J. Am. Chem. Soc.* **1979**, *101*, 6754−6756.
(18) Grate, J. H.; Schrauzer, G. N. Chemistry of Cobalamins and Related Compounds. 48. Sterically Induced, Spontaneous Dealkylation of Secondary Alkylcobalamins Due to Axial Base Coordination and Conformational Changes of the Corrin Ligand. *J. Am. Chem. Soc.* **1979**, *101*, 4601−4611.
(19) Pang, J.; Li, X.; Morokuma, K.; Scrutton, N. S.; Sutcliffe, M. J. Large-Scale Domain Conformational Change Is Coupled to the Activation of the Co−C Bond in the B_{12}-Dependent Enzyme Ornithine 4,5-Aminomutase: A Computational Study. *J. Am. Chem. Soc.* **2012**, *134*, 2367−2377.
(20) Shaik, S.; Cohen, S.; Wang, Y.; Chen, H.; Kumar, D.; Thiel, W. P450 Enzymes: Their Structure, Reactivity, and Selectivity-Modeled by QM/MM Calculations. *Chem. Rev.* **2010**, *110*, 949−1017.
(21) Patra, R.; Sahoo, D.; Dey, S.; Sil, D.; Rath, S. P. Switching Orientation of Two Axial Imidazole Ligands between Parallel and Perpendicular in Low-Spin Fe(III) and Fe(II) Nonplanar Porphyrinates. *Inorg. Chem.* **2012**, *51*, 11294−11305.
(22) Patra, R.; Chaudhary, A.; Ghosh, S. K.; Rath, S. P. Axial Ligand Orientations in a Distorted Porphyrin Macrocycle: Synthesis, Structure, and Properties of Low-Spin Bis(imidazole)iron(III) and Iron(II) Porphyrinates. *Inorg. Chem.* **2010**, *49*, 2057−2067.
(23) Patra, R.; Bhowmik, S.; Ghosh, S. K.; Rath, S. P. Effects of Axial Pyridine Coordination on a Saddle-Distorted Porphyrin Macrocycle: Stabilization of Hexa-Coordinated High-Spin Fe(III) and Air-Stable Low-Spin Iron(II) Porphyrinates. *Dalton Trans.* **2010**, *39*, 5795−5806.
(24) Zoppellaro, G.; Harbitz, E.; Kaur, R.; Ensign, A. A.; Bren, K. L.; Andersson, K. K. Modulation of the Ligand-Field Anisotropy in a Series of Ferric Low-Spin Cytochrome *c* Mutants derived from *Pseudomonas aeruginosa* Cytochrome *c*-551 and *Nitrosomonas europaea* Cytochrome *c*-552: A Nuclear Magnetic Resonance and Electron Paramagnetic Resonance Study. *J. Am. Chem. Soc.* **2008**, *130*, 15348−15360.
(25) Teschner, T.; Yatsunyk, L.; Schünemann, V.; Paulsen, H.; Winkler, H.; Hu, C.; Scheidt, W. R.; Walker, F. A.; Trautwein, A. X. Models of the Membrane-Bound Cytochromes: Mössbauer Spectra of Crystalline Low-Spin Ferriheme Complexes Having Axial Ligand Plane Dihedral Angles Ranging from 0° to 90°. *J. Am. Chem. Soc.* **2006**, *128*, 1379−1389.
(26) Shao, J.; Steene, E.; Hoffman, B. M.; Ghosh, A. EPR, ENDOR, and DFT Studies on (*β*-Octahalo-meso-tetraarylporphyrin)copper Complexes: Characterization of the Metal($d_{x^2-y^2}$)−Porphyrin(a_{2u}) Orbital Interaction. *Eur. J. Inorg. Chem.* **2005**, *2005*, 1609−1615.
(27) Christoforidis, K. C.; Louloudi, M.; Milaeva, E. R.; Deligiannakis, Y. Mechanism of Catalytic Decomposition of Pentachlorophenol by a Highly Recyclable Heterogeneous SiO_2−[Fe-Porphyrin] Catalyst. *J. Catal.* **2010**, *270*, 153−162.
(28) Zhou, Z. C.; Zhang, X.; Liu, Q. H.; Yan, Z. Q.; Lv, C. J.; Long, G. Geometry and Temperature Dependence of meso-Aryl Rotation in Strained Metalloporphyrins: Adjustable Turnstile Molecules. *Inorg. Chem.* **2013**, *52*, 10258−10263.
(29) Geno, M. K.; Halpern, J. Why Does Nature Not Use the Porphyrin Ligand in Vitamin B_{12}? *J. Am. Chem. Soc.* **1987**, *109*, 1238−1240.
(30) Zhou, Z. C.; Shen, M.; Cao, C. Z.; Liu, Q. H.; Yan, Z. Q. Opposing Influences of Ruffling and Doming Deformation on the 4-N Cavity Size of Porphyrin Macrocycles: The Role of Heme Deformations Revealed. *Chem. - Eur. J.* **2012**, *18*, 7675−7679.
(31) Zhou, Z. C.; Cao, C. Z.; Liu, Q. H.; Jiang, R. Q. Hybrid Orbital Deformation (HOD) Effect and Spectral Red-Shift Property of Nonplanar Porphyrin. *Org. Lett.* **2010**, *12*, 1780−1783.
(32) Zhou, Z. C.; Liu, Q. H.; Yan, Z. Q.; Long, G.; Zhang, X.; Cao, C.; Jiang, R. Q. Conversion of Electron Configuration of Iron Ion through Core Contraction of Porphyrin: Implications for Heme Distortion. *Org. Lett.* **2013**, *15*, 606−609.
(33) Liu, Q. H.; Zhou, X. C.; Liu, H. M.; Zhang, X.; Zhou, Z. C. Fractional Transfer of a Free Unpaired Electron to Overcome Energy Barriers in the Formation of Fe^{4+} from Fe^{3+} during the Core Contraction of Macrocycles: Implication for Heme Distortion. *Org. Biomol. Chem.* **2015**, *13*, 2939−2946.
(34) Zhou, Z. C.; Zhou, X. C.; Liu, Q. H.; Zhang, X.; Liu, H. M. Fixation of Zinc(II) Ion to Dioxygen in a Highly Deformed Porphyrin: Implications for the Oxygen Carrier Mechanism of Distorted Heme. *Org. Lett.* **2015**, *17*, 4078−4081.
(35) Newcomb, M.; Zhang, R.; Chandrasena, R. E. P.; Halgrimson, J. A.; Horner, J. H.; Makris, T. M.; Sligar, S. G. Cytochrome P450 Compound I. *J. Am. Chem. Soc.* **2006**, *128*, 4580−4581.
(36) Jeandon, C.; Ruppert, R.; Callot, H. J. Acylation of Nickel meso-Tetraarylporphyrins: Porphyrin to Corrole Ring Contraction and Formation of seco-Porphyrins. *J. Org. Chem.* **2006**, *71*, 3111−3120.
(37) Haynes, W. M. *Handbook of Chemistry and Physics*, 91st ed.; CRC Press: Boca Raton, FL, 2010; section 9, p 18, and section 12, p 11.
(38) Paolesse, R.; Licoccia, S.; Bandoli, G.; Dolmella, A.; Boschi, T. First Direct Synthesis of a Corrole Ring from a Monopyrrolic Precursor. Crystal and Molecular Structure of (Triphenylphosphine)-(5,10,15-triphenyl-2,3,7,8,12,13,17,18-octamethylcorrolato)cobalt-(III)-Dichloromethane. *Inorg. Chem.* **1994**, *33*, 1171−1176.
(39) Randaccio, L.; Furlan, M.; Geremia, S.; Slouf, M.; Srnova, I.; Toffoli, D. Similarities and Differences between Cobalamins and Cobaloximes. Accurate Structural Determination of Methylcobalamin and of LiCl- and KCl-Containing Cyanocobalamins by Synchrotron Radiation. *Inorg. Chem.* **2000**, *39*, 3403−3413.
(40) Sparapany, J. W.; Crossley, M. J.; Baldwin, J. E.; Ibers, J. A. Structure of the Cobalt(II)-"Capped" Porphyrin, Co(C_3-Cap).3$CHCl_3$. *J. Am. Chem. Soc.* **1988**, *110*, 4559−4564.
(41) Venkatasubbaiah, K.; Zhu, X. J.; Kays, E.; Hardcastle, K. I.; Jones, C. W. Co(III)-Porphyrin-Mediated Highly Regioselective Ring-Opening of Terminal Epoxides with Alcohols and Phenols. *ACS Catal.* **2011**, *1*, 489−492.
(42) Kadish, K. M.; Frémond, L.; Ou, Z.; Shao, J.; Shi, C.; Anson, F. C.; Burdet, F.; Gros, C. P.; Barbe, J.-M.; Guilard, R. Cobalt(III)

DOI: 10.1021/acs.jpcb.5b08431
J. Phys. Chem. B 2015, 119, 14102−14110

Corroles as Electrocatalysts for the Reduction of Dioxygen: Reactivity of a Monocorrole, Biscorroles, and Porphyrin−Corrole Dyads. *J. Am. Chem. Soc.* **2005**, *127*, 5625−5631.
(43) Erben, C.; Will, S.; Kadish, K. M. In *The Porphyrin Handbook*; Kadish, K. M., Smith, K. M., Guilard, R., Eds.; Academic Press: Boston, 2000; Vol. *2*, pp 233−300.
(44) Simonis, U.; Walker, F. A.; Lee, P. L.; Hanquet, B. J.; Meyerhoff, D. J.; Scheidt, W. R. Synthesis, Spectroscopic, and Structural Studies of Extremely Short Chain Basket Handle Porphyrins and Their Zinc(II) Complexes. *J. Am. Chem. Soc.* **1987**, *109*, 2659−2668.
(45) Adler, A. D.; Longo, F. R.; Kampas, F.; Kim, J. On the Preparation of Metalloporphyrins. *J. Inorg. Nucl. Chem.* **1970**, *32*, 2443−2445.
(46) Shelnutt, J. A.; Song, X. Z.; Ma, J. G.; Jia, S. L.; Jentzen, W.; Medforth, C. J. Nonplanar Porphyrins and Their Significance in Proteins. *Chem. Soc. Rev.* **1998**, *27*, 31−42.
(47) Kulcsár, Á.; Saltiel, J.; Zimányi, L. Dissecting the Photocycle of the Bacteriorhodopsin E204Q Mutant from Kinetic Multichannel Difference Spectra. Extension of the Method of Singular Value Decomposition with Self-Modeling to Five Components. *J. Am. Chem. Soc.* **2001**, *123*, 3332−3340.
(48) Picaud, T.; Le Moigne, C.; Loock, B.; Momenteau, M.; Desbois, A. Nonplanar Distortions of Bis-Base Low-Spin Iron(II)−Porphyrinates: Absorption and Resonance Raman Investigations of Cross-Trans-Linked Iron(II)−Basket-Handle Porphyrin Complexes. *J. Am. Chem. Soc.* **2003**, *125*, 11616−11625.
(49) Duval, H.; Bulach, V.; Fischer, J.; Weiss, R. Four-Coordinate, Low-Spin (S = 0) and Six-Coordinate, High-Spin (S = 1) Nickel(II) Complexes of Tetraphenylporphyrins with *β*-Pyrrole Electron-Withdrawing Substituents: Porphyrin-Core Expansion and Conformation. *Inorg. Chem.* **1999**, *38*, 5495−5501.
(50) Renner, M. W.; Barkigia, K. M.; Melamed, D.; Gisselbrecht, J.-P.; Nelson, N. Y.; Smith, K. M.; Fajer, J. Conformational Control of Oxidation Sites, Spin States and Orbital Occupancy in Nickel Porphyrins. *Res. Chem. Intermed.* **2002**, *28*, 741−759.
(51) Shannon, R. D. Revised Effective Ionic Radii and Systematic Studies of Interatomic Distances in Halides and Chalcogenides. *Acta Crystallogr., Sect. A: Cryst. Phys., Diffr., Theor. Gen. Crystallogr.* **1976**, *32*, 751−767.
(52) Singh, R.; Switala, J.; Loewen, P. C.; Ivancich, A. Two [Fe(IV) = O Trp•] Intermediates in M. Tuberculosis Catalase-Peroxidase Discriminated by Multifrequency (9−285 GHz) EPR Spectroscopy: Reactivity toward Isoniazid. *J. Am. Chem. Soc.* **2007**, *129*, 15954−15963.
(53) Ghosh, S. K.; Patra, R.; Rath, S. P. Axial Ligand Coordination in Sterically Strained Vanadyl Porphyrins: Synthesis, Structure, and Properties. *Inorg. Chem.* **2008**, *47*, 9848−9856.
(54) Patra, R.; Chaudhary, A.; Ghosh, S. K.; Rath, S. P. Modulation of Metal Displacements in a Saddle Distorted Macrocycle: Synthesis, Structure, and Properties of High-Spin Fe(III) Porphyrins and Implications for the Hemoproteins. *Inorg. Chem.* **2008**, *47*, 8324−8335.
(55) Walker, F. A. An Electron Spin Resonance Study of Coordination to the Fifth and Sixth Positions of *α,β,γ,δ*-Tetra (pmethoxypheny1)porphinatocobalt (II). *J. Am. Chem. Soc.* **1970**, *92*, 4235−4244.
(56) Deeth, R. J. Saddle Distortions of Ferryl-Porphyrin Models for Peroxidase Compound I: A Density Functional Study. *J. Am. Chem. Soc.* **1999**, *121*, 6074−6075.
(57) Nakamura, M.; Ohgo, Y.; Ikezaki, A. Electronic Ground States of Low-Spin Iron(III) Porphyrinoids. *J. Inorg. Biochem.* **2008**, *102*, 433−445.
(58) Patra, R.; Bhowmik, S.; Ghosh, S. K.; Rath, S. P. Effects of Axial Pyridine Coordination on a Saddle-Distorted Porphyrin Macrocycle: Stabilization of hexa-Coordinated High-Spin Fe(III) and Air-Stable Low-Spin Iron(II) Porphyrinates. *Dalton Trans.* **2010**, *39*, 5795−5806.
(59) Cheng, R.-J.; Wang, Y.-K.; Chen, P.-Y.; Han, Y.-P.; Chang, C.-C. An Unexpected Bonding Interaction between d_{xy} and a_{1u} Orbitals Mediated by Porphyrin Deformation. *Chem. Commun.* **2005**, 1312−1314.
(60) Walker, F. A. ESR Studies of Co(II) Tetraphenylporphyrins and Their Oxygen Adducts: Complex Formation with Aromatic Molecules and Sterically Hindered Lewis Bases. *J. Magn. Reson. (1969-1992)* **1974**, *15*, 201−218.
(61) Banci, L.; Bencini, A.; Benelli, C.; Gatteschi, D.; Zanchini, C. Spectral-Structural Correlations in High-Spin Cobalt(II) Complexes. *Struct. Bonding (Berlin)* **1982**, *52*, 37−86.
(62) Gaffney, B. J.; Silverstone, H. J. In *Biological Magnetic Resonance EMR of Paramagnetic Molecules*; Berliner, L. J., Reuben, J., Eds.; Plenum Press: New York, 1993; Vol. *13*, pp 1−55.
(63) Satoh, M.; Ohba, Y.; Yamauchi, S.; Iwaizumi, M. Temperature- and Axial-Ligand-Dependent EPR Spectra of Cobalt Porphyrin Cation Radicals: Effects of Mixing of the A_{1u}, and A_{2u}, States and a Locally Excited Triplet State. *Inorg. Chem.* **1992**, *31*, 298−303.
(64) Hirota, S.; Polson, S. M.; Puckett, J. M., Jr.; Moore, S. J.; Mitchell, M. B.; Marzilli, L. G. The Co−CH_3 Bond in Imine/Oxime B_{12} Models. Influence of the Orientation and Donor Properties of the trans Ligand As Assessed by FT-Raman Spectroscopy. *Inorg. Chem.* **1996**, *35*, 5646−5653.
(65) Brucker, E. A.; Olson, J. S.; Phillips, G. N., Jr; Dou, Y.; Ikeda-Saito, M. High Resolution Crystal Structures of the Deoxy, Oxy, and Aquomet Forms of Cobalt Myoglobin. *J. Biol. Chem.* **1996**, *271*, 25419−25422.
(66) Lacy, D. C.; Park, Y. J.; Ziller, J. W.; Yano, J.; Borovik, A. S. Assembly and Properties of Heterobimetallic $Co^{II/III}/Ca^{II}$ Complexes with Aquo and Hydroxo Ligands. *J. Am. Chem. Soc.* **2012**, *134*, 17526−17535.
(67) Olea, C.; Kuriyan, J.; Marletta, M. A. Modulating Heme Redox Potential through Protein-Induced Porphyrin Distortion. *J. Am. Chem. Soc.* **2010**, *132*, 12794−12795.
(68) Kadish, K. M. The Electrochemistry of Metalloporphyrins in Nonaqueous Media. *Prog. Inorg. Chem.* **1986**, *34*, 435−605.
(69) Zou, S.; Clegg, R. S.; Anson, F. C. Attachment of Cobalt "Picket Fence" Porphyrin to the Surface of Gold Electrodes Coated with 1-(10-Mercaptodecyl)imidazole. *Langmuir* **2002**, *18*, 3241−3246.
(70) Guilard, R.; Gros, C. P.; Bolze, F.; Jérôme, F.; Ou, Z.; Shao, J.; Fischer, J.; Weiss, R.; Kadish, K. M. Alkyl and Aryl Substituted Corroles. 1. Synthesis and Characterization of Free Base and Cobalt Containing Derivatives. X-ray Structure of $(Me_4Ph_5Cor)Co(py)_2$. *Inorg. Chem.* **2001**, *40*, 4845−4855.

DOI: 10.1021/acs.jpcb.5b08431
J. Phys. Chem. B 2015, 119, 14102−14110